Advances in Water Resources 166 (2022) 104258

Contents lists available at ScienceDirect

Advances in Water Resources

journal homepage: www.elsevier.com/locate/advwatres

Mapping storm spatial profiles for flood impact assessments

Nadav Peleg [a,*], Nikolina Ban [b], Michael J. Gibson [c], Albert S. Chen [c], Athanasios Paschalis [d], Paolo Burlando [e], João P. Leitão [f,*]

[a] Institute of Earth Surface Dynamics, University of Lausanne, 1015 Lausanne, Switzerland
[b] Department of Atmospheric and Cryospheric Sciences, University of Innsbruck, 6020 Innsbruck, Austria
[c] The Centre for Water Systems, University of Exeter, EX4 4QF Exeter, United Kingdom
[d] Department of Civil and Environmental Engineering, Imperial College London, SW7 2AZ London, United Kingdom
[e] Institute of Environmental Engineering, ETH Zurich, 8093 Zurich, Switzerland
[f] Department of Urban Water Management, Swiss Federal Institute of Aquatic Science and Technology, 8600 Dubendorf, Switzerland

ARTICLE INFO

Keywords:
Spatial quantile mapping
Extreme rainfall
Urban flood
High-resolution rainfall
Climate change

ABSTRACT

Synthetic design storms are often used to plan new drainage systems or assess flood impacts on infrastructure. To simulate extreme rainfall events under climate change, design storms can be modified to match a different return frequency of extreme rainfall events as well as a modified temporal distribution of rainfall intensities. However, the same magnitude of change to the rainfall intensities is often applied in space. Several hydrological applications are limited by this. Climate change impacts on urban pluvial floods, for example, require the use of 2D design storms (rainfall fields) at sub-kilometer and sub-hourly scales. Recent kilometer scale climate models, also known as convection-permitting climate models (CPM), provide rainfall outputs at a high spatial resolution, although rainfall simulations are still restricted to a limited number of climate scenarios and time periods. We nevertheless explored the potential use of rainfall data obtained from these models for hydrological flood impact studies by introducing a method of spatial quantile mapping (SQM). To demonstrate the new methodology, we extracted high-resolution rainfall simulations from a CPM for four domains representing different urban areas in Switzerland. Extreme storms that are plausible under the present climate conditions were simulated with a 2D stochastic rainfall model. Based on the CPM-informed stochastically generated rainfall fields, we modified the design storms to fit the future climate scenario using three different methods: the SQM, a uniform quantile mapping, and a uniform adjustment based on a rainfall–temperature relationship. Throughout all storms, the temporal distribution of rainfall was the same. Using a flood model, we assessed the impact of different rainfall adjustment methods on urban flooding. Significant differences were found in the flood water depths and areas between the three methods. In general, the SQM method results in a higher flood impact than the storms that were modified otherwise. The results suggest that spatial storm profiles may need to be re-adjusted when assessing flood impacts.

1. Introduction

Floods are one of the main natural hazards contributing to massive economic losses and casualties (Paprotny et al., 2018). Especially vulnerable to damage from river overflows and flash floods are urban areas, which contain significant concentrations of infrastructure including residential, commercial, and industrial structures (Gueneralp et al., 2015). Flash floods are commonly triggered by short-duration but intense rainfall bursts (e.g. Fowler et al., 2021b); while river overflows are caused primarily by prolonged rainfall events (and other climate factors, such as snow-melt and evaporation, see Bloeschl et al., 2019). Global warming is predicted to cause both short- and long-duration extreme rainfall events to occur more frequently and with greater intensity in the future (Trenberth, 2011; Westra et al., 2014; Moustakis et al., 2021; Fowler et al., 2021a). Consequently, higher flood-frequencies, damages, and economic losses are predicted (Hirabayashi et al., 2013; Jongman et al., 2014; Mallakpour and Villarini, 2015).

Design storms are a commonly used tool for assessing flood impacts (Sun et al., 2011). They are often synthetic hyetographs that represent extreme rainfall events for a given return period and storm duration (Berk et al., 2017). Hyetographs can either have a simple bell-like shape with a length and maximum rainfall intensity matching observed extreme rainfall events, or they can be stochastically modeled

* Corresponding authors.
E-mail addresses: nadav.peleg@unil.ch (N. Peleg), joaopaulo.leitao@eawag.ch (J.P. Leitão).

https://doi.org/10.1016/j.advwatres.2022.104258
Received 1 February 2022; Received in revised form 22 May 2022; Accepted 19 June 2022
Available online 25 June 2022

to simulate pseudo extreme rainfall events (Onof et al., 2000; Chimene and Campos, 2020). On the basis of climate model data, their intensities can be adapted to reflect extreme rainfall events at future climates (e.g Berggren et al., 2014; Peleg et al., 2015).

Design storms can be conceptualized at a point scale [i.e. in a one-dimensional (1D) spatial configuration], representing the areal rainfall over a catchment (Onof et al., 2000). In some circumstances, however, using design storms with a two-dimensional (2D) configuration is more appropriate (e.g. Paschalis et al., 2014; Niemi et al., 2016; Peleg et al., 2020); especially when extreme rainfall events are convective in nature, as they often exhibit a high degree of spatial heterogeneity (Belachsen et al., 2017). Additionally, fast-response catchments, such as those in mountainous or urban areas, are sensitive to rainfall heterogeneity (Peleg et al., 2017a; Moraga et al., 2021), making spatially distributed simulations necessary. Another advantage of using stochastic models to simulate design storms is that their output is an ensemble of multiple space–time realizations of the storm. Since stochastic space–time variability is a significant source of uncertainty in hydrological impacts (Fatichi et al., 2016; Peleg et al., 2017a; Moraga et al., 2021), it is beneficial to simulate it in order to, for example, evaluate the effects of climate change on changes in storm properties on flood statistics. A number of stochastic models are available to simulate 2D design storms. These include the STREAP model (Paschalis et al., 2013), the HiReS-WG (Peleg and Morin, 2014), and the STORM model (Singer et al., 2018), among others.

In many locations, we can estimate how the magnitude, duration and temporal structure of storm hyetographs will likely change under future climate conditions. Climate models can provide this type of information or it can be obtained from empirical relationships between extreme rainfall properties and climate variables, such as temperature increase (Ban et al., 2014; Wasko and Sharma, 2015; Li et al., 2018; Moustakis et al., 2020; Ali et al., 2021). It is possible to modify 1D design storms for climate change impact studies when this information is available (e.g. Olsson et al., 2013).

Global warming is also projected to change the spatial patterns of extreme rainfall. A number of studies linked changes in temperature to changes in storm extent and spatial heterogeneity of rainfall fields (Wasko et al., 2016; Lochbihler et al., 2017; Peleg et al., 2018; Chen et al., 2021). Climate-induced changes in the spatial properties of extreme rainfall have been found to influence catchment hydrological responses (Peleg et al., 2020, 2021). As a result, when using 2D design storms, it is crucial not only to modify the rainfall intensities and temporal structure but also the spatial structure of the storm.

Convection-permitting climate models (CPM) can simulate rainfall fields at high spatial and temporal resolution (i.e. on kilometers and sub-hour scales, Prein et al., 2015; Schär et al., 2020). As a result of their high computational demand and the time required to run them, CPM are not currently used to simulate a wide range of emissions scenarios for long periods of time (e.g. simulating the entire 21st century). Thus, CPM data tend to underrepresent low-frequency intense storms. Consequently, in the vast majority of cases, their data cannot be used directly for hydrological flood assessment studies. Their data can be used to understand how, for example, rainfall intensities are affected by air temperatures (Lenderink et al., 2021), allowing design storms to be adjusted accordingly. Based on their ability to explicitly simulate deep convection, these models have proven to reproduce the spatial structure of rainfall adequately at the kilometer-scale for numerous areas (Ban et al., 2014, 2021; Leutwyler et al., 2017), including over

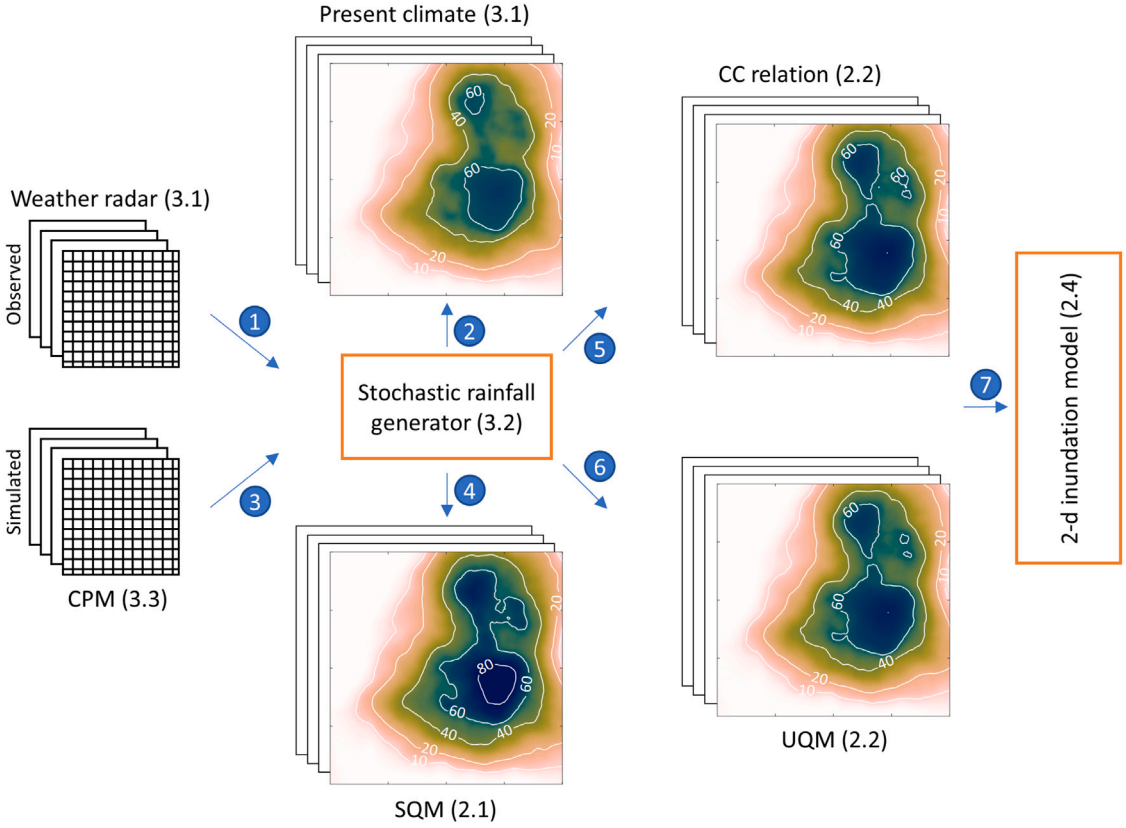

Fig. 1. An illustration of the steps taken in the study. The spatio-temporal characteristics of an extreme rainfall event are derived from weather radar and parameterized in a stochastic rainfall generator (1). On the basis of this parameterization, a design storm that represents an extreme event for the present climate is simulated (2). With a convection-permitting model (CPM), the changes to extreme rainfall intensities, temperatures during extreme rainfall events, and the spatial structure of extreme rainfall between present and future periods are analyzed (3). The design storm is modified and simulated for future climate conditions using the spatial quantile mapping (SQM, 4) method, the rainfall–temperature relationship method (CC, 5), and the uniform quantile mapping (UQM, 6) method. The design storms (present and future) are used as inputs to a 2D flood inundation model (7). The relevant section of the paper is indicated in brackets and the colors indicate rainfall intensity from low (brownish) to high (dark blue).

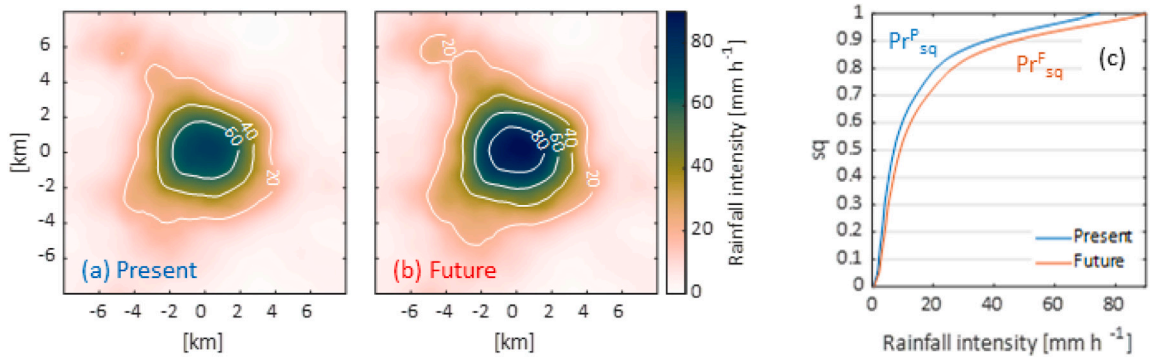

Fig. 2. An example of a present (a) and future (b) storm composite (see Section 2.1) obtained from a CPM. The cumulative distribution functions of the spatial rainfall intensities of the composites are presented in (c), where sq is the spatial quantile.

complex terrain (e.g. Lind et al., 2020). In the context of climate change, CPM can be used to investigate how the spatial structure of extreme storms will change in the future (e.g. Prein et al., 2017, 2020; Chen et al., 2021). While theoretically this information can be used to alter the spatial structure of 2D design storms for flood assessment applications, in practice this has not been done yet.

In this paper, we describe a new spatial quantile mapping technique that allows for the modification of the spatial structure of 2D design storms. The extreme storm observed in Lausanne in summer 2018 served as our case study in order to construct a 2D design storm and modify its spatial structure to fit future climate conditions. With our 2D modified design storm, we examined flood statistics in four Swiss cities using a flood inundation model and discuss the importance of modifying the spatial structure of storms by comparing our new method with other widely-used methods that allow changes in storm magnitude but lack the spatial dimension.

2. Rainfall adjustment methods

We simulated a 2D design storm, altered it spatially to take into account the modifications expected due to climate change, and examined the changes in flood statistics. In addition, we also tested two other non-spatial rainfall modification methods. These processes are illustrated and explained in Fig. 1; the methods for modifying the rainfall patterns and intensity are explained in the subsequent subsections, and the numerical experiment we conducted as a case study is described in Section 3.

2.1. Spatial quantile mapping

The initial step in performing the spatial quantile mapping (SQM) method is to calculate storm composites using the CPM, both for storms occurring in the present climate (Fig. 2a) and future climate (Fig. 2b). The choice of storms to include depends on the application. Suppose the aim is to modify a design storm that represents a 10-year return period; the relevant rain fields for this return period should then be extracted from an archive of present and future CPM simulations. The storm composite is constructed by centering each rainfall field from the 10-year storm archive on the location of their maximum rainfall intensity over one another and calculating the mean of the rainfall intensities at each grid cell. We assume that the spatial structure of the storm composite is stationary, and that the adjustment factors derived from the composite can be applied to each distinct rainfall field of the design storm.

The empirical cumulative distribution function (CDF) of the spatial rainfall intensities of the present and future storms is then compiled (Fig. 2c). The rainfall intensities obtained from the storm composites are sorted and linearly ranked from the lowest rainfall intensity ($sq = 0$) to the highest ($sq = 1$). Linear interpolation is used to compute rain intensity continuous over the entire quantile ranges, $sq \in [0, 1]$. In most cases, it is possible to fit a probability distribution to the data, instead of the empirical CDF; for example, the rain fields presented in Fig. 2 can be fitted with a lognormal distribution, which is a common probability distribution in rain fields (e.g. Cho et al., 2004). In order to calculate the adjustment factor of rainfall intensity per quantile (CF_{sq}), we divide the future storm profile, Pr^F_{sq}, by the present storm profile, Pr^P_{sq} (both are illustrated in Fig. 2c):

$$CF_{sq} = \frac{Pr^F_{sq}}{Pr^P_{sq}}, \tag{1}$$

The adjustment factor can then be applied to adjust the rainfall intensities of the design storm:

$$R^F_{i,sq} = R^P_{i,sq} \cdot CF_{sq}, \tag{2}$$

where i are the individual rain fields composing the design storm R.

In addition to changes in rainfall intensity, it is likely that the area of the storm will change in the future. Adjusting the area of the storm is therefore also necessary and should be applied per rainfall field. It is essential to know which probability distribution the rainfall intensities follow in space in order to perform the adjustment. The area adjustment procedure is done as follows: (i) the rainfall intensity field is transformed into its quantile field; (ii) a random quantile vector is generated, with the size of the "wet" number of grid cells representing the new area; (iii) in the quantile field, "dry" grid cells that are close to "wet" grid cells (by euclidean distance) are converted into "wet" grid cells so as to reach the desired storm area; (iv) the quantiles from the second step are assigned to the quantile field; and (v) the quantile field is back-transformed into a rainfall intensity field. Using this procedure, the area of the rainfall field can be modified while the storm spatial structure remains largely intact. In the case of shrinking fields, the same procedure can be applied but in step (iii) the grid cells with the lowest rainfall intensities are classified as "dry" until the desired rainfall area is met.

As an example, we used a rainfall field characterized by a spatial lognormal distribution (Fig. 3a). The following parameters can be derived from this synthetic rainfall field: the mean areal rainfall ($\hat{R}$), the total wetted area (R_a), and the spatial rainfall coefficient of variation (R_{cv}). Based on this information, the rainfall field can be transformed into its quantile field (Fig. 3b) using the following transformation (see Paschalis et al., 2013; Peleg et al., 2020, for details):

$$Q(x,y) = LN\left(R(x,y), log\left(\frac{R_a}{\sqrt{R^2_{cv}+1}}\right), \sqrt{log(R^2_{cv}+1)}\right), \tag{3}$$

where $Q(x, y)$ is the quantile field obtained from the LN cumulative lognormal distribution; $R(x, y)$ is the rainfall intensity field,

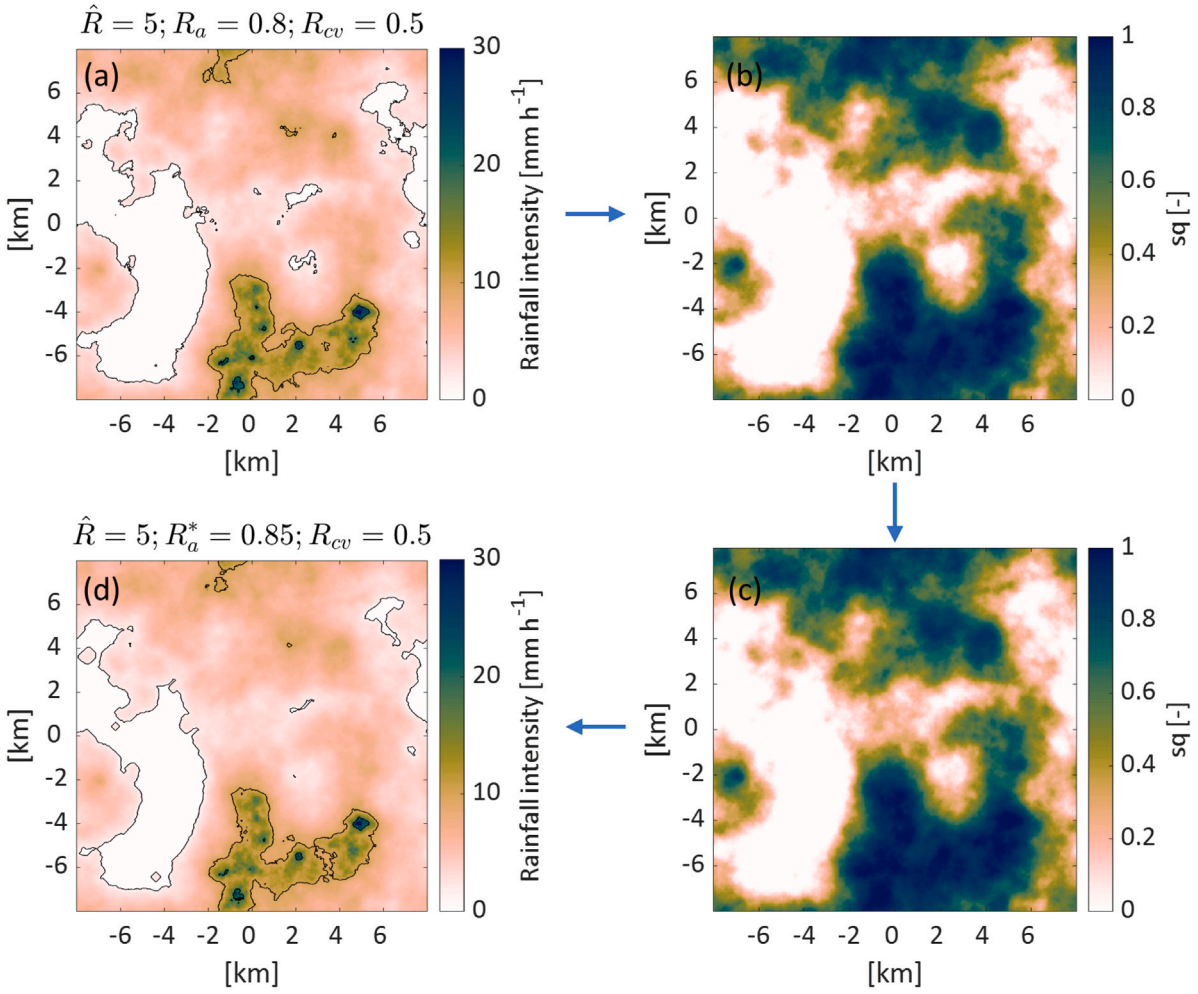

Fig. 3. (a) A rainfall field with a lognormal spatial distribution of rainfall intensities. From the field, the mean areal rainfall ($\hat{R}$), the total wetted area (R_a), and the spatial rainfall coefficient of variation (R_{cv}) are calculated. (b) is the quantile field of (a). (c) is a new quantile field with an increased wetted area (see Section 2.1 for details). In (d), the quantile field (c) is converted back to the rainfall intensity field.

$log\left(\frac{R_a}{\sqrt{R_{cv}^2+1}}\right)$ is the μ parameter, and $\sqrt{log(R_{cv}^2+1)}$ is the σ parameter of the probability distribution.

The next step is to generate the quantile vector Q_N with a length that correspond to the number of grid cells of the newly desired area:

$$Q_N = N^{-1}\left[\sim N(0,1), 0, 1\right], \tag{4}$$

where N^{-1} is the inverse cumulative normal distribution and $\sim N$ is a randomly generated Normal vector (a zero-mean, unit-variance Gaussian). The length of Q_N determines the new area of the rainfall field (R_a^*) and is defined as $R_a^* = R_a\, CF_a$; where CF_a is the adjustment factor of the total wetted area, obtained from dividing the future total wetted area of the rainfall composite with the present one. Using a simple image morphological dilation method (e.g. van den Boomgaard and van Balen, 1992), the quantile field $[Q(x,y)]$ is then adjusted to match the desired area, and the values of the simulated vector (Q_N) are sorted similarly to the original field and assigned to the newly adjusted quantile field $[Q^*(x,y)]$ (Fig. 3c). By using a morphological method to adjust the wetted area, we assume that the spatial correlation structure of the rainfall field is approximately stationary, i.e. changes in the spatial correlation structure due to climate change are not explicitly accounted for.

The newly adjusted quantile field is finally back-transformed into a rainfall intensity field:

$$R^*(x,y) = LN^{-1}\left(Q^*(x,y), log\left(\frac{R_a^*}{\sqrt{R_{cv}^2+1}}\right), \sqrt{log(R_{cv}^2+1)}\right), \tag{5}$$

where $R^*(x,y)$ is the new rainfall intensity field (Fig. 3d), $Q^*(x,y)$ is the adjusted quantile field (Fig. 3c), and LN^{-1} is the inverse cumulative lognormal distribution.

The above example used the lognormal distribution, but the same procedure can be applied to any probability distribution.

2.2. Other rainfall adjustment methods

The two other non-spatial rainfall modification methods that were used here are a uniform adjustment based on a rainfall–temperature relationship (CC relation) and uniform quantile mapping (UQM) methods (Fig. 1). The first is based on the well-known Clausius–Clapeyron relation (Trenberth et al., 2003) that link extreme rainfall intensification (mostly convective in type) and increase in temperature (see recent publications by Moustakis et al., 2020; Ali et al., 2021; Fowler et al., 2021a, among many others). Based on the assumption that the rainfall will intensify at a rate of 7% °C^{-1} (a valid assumption for

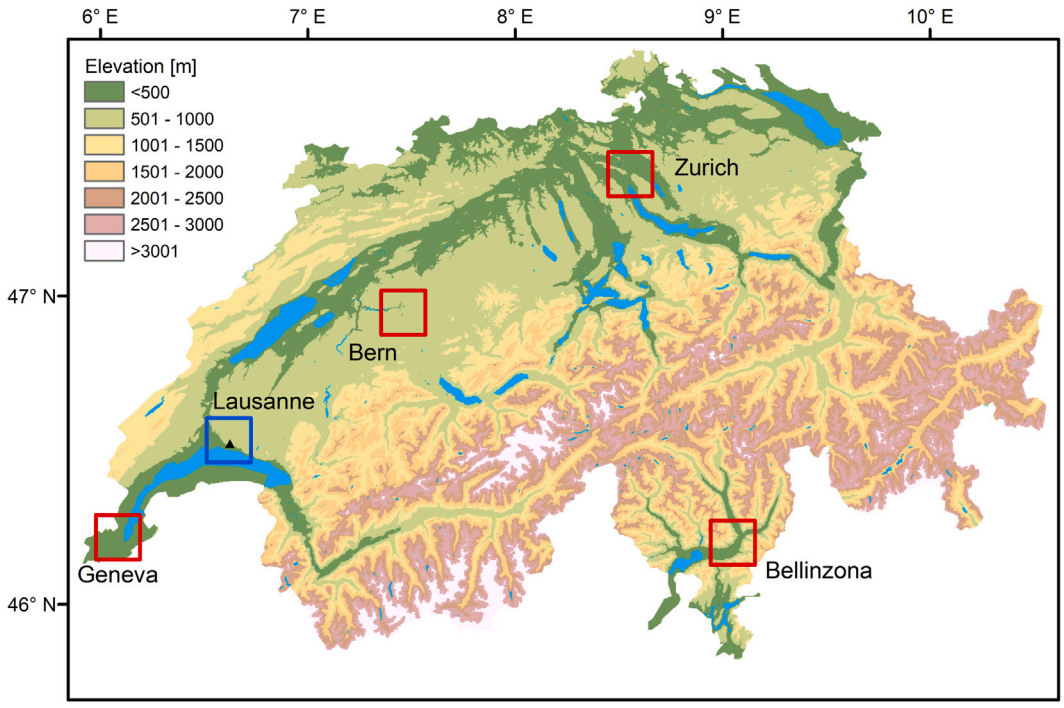

Fig. 4. A map of Switzerland with the locations of Geneva, Bern, Zurich, Bellinzona (red squares), and Lausanne (blue square). Each square is 16 km x 16 km. A black triangle marks the location of the Lausanne (LSN) rain gauge.

Switzerland; Molnar et al., 2015; Ban et al., 2015), we defined the rainfall intensification factor as follows:

$$CC = 1.07^{T}, \tag{6}$$

where CC is the "Clausius–Clapeyron" intensification factor that is determined by the increase in temperature T. The new rainfall field $R^{*}(x, y)$ is simply a multiplication of $R(x, y)$ with CC.

The UQM is expressed as:

$$R^{*}(x, y) = F^{-1}\left[U\left(R(x, y)\right)\right], \tag{7}$$

where U is the quantile function and F^{-1} is an inverse cumulative probability distribution function. We used the generalized Pareto distribution in our case study (as in Peleg et al., 2017b). It was fitted to the CPM's rainfall intensities of the present climate (replacing U) and of the future climate (replacing F^{-1}).

3. Modifying an intense storm: a case study

The numerical experiment is illustrated in Fig. 1. As our case study, we selected the extreme storm recorded over the city of Lausanne (Section 3.1). Applying a stochastic rainfall generator model, we simulated multiple realizations of this storm (Section 3.2). Then, we evaluated the abilities of CPM to generate extreme rainfall in this region (Section 3.3) and determined how the spatial structure of the storm is expected to change (Section 3.4). We duplicated the "Lausanne storm" for four other cities in Switzerland (Fig. 4), which are considerably larger than Lausanne, and modified its spatial structure using the methods listed in Section 2. The selected cities are located in different climatic zones with different urban forms and terrain characteristics, thus representing a wide variety of urban hydrological responses to extreme rainfall. As a final step, we used an inundation model (Section 3.5) to examine the hydrological response.

3.1. The "Lausanne storm"

On June 11th, 2018, an intense convective storm swept through the city of Lausanne in Switzerland (Fig. 4). The storm lasted for four hours, between 7 PM and 11 PM local time, and is the most intense short rain burst ever recorded in Switzerland. At around 9 pm, a rain gauge in the city's vicinity (LSN) recorded a peak of 41 mm of rainfall within 10 min (Fig. 5). The rain burst flooded several streets and the underground metro system, causing damage but no casualties.

The storm was captured not only by the local rain gauge but also by the MeteoSwiss weather radar system, which enabled the analysis of the space–time evolution of the storm at a fine resolution of 1 km and 5 min (Germann et al., 2015). A 16 km x 16 km window centered over Lausanne was used to analyze the storm's mean areal rainfall intensity ($\hat{R}$), rainfall spatial structure (R_{cv}), and fraction of wetted area (R_a, Fig. 5).

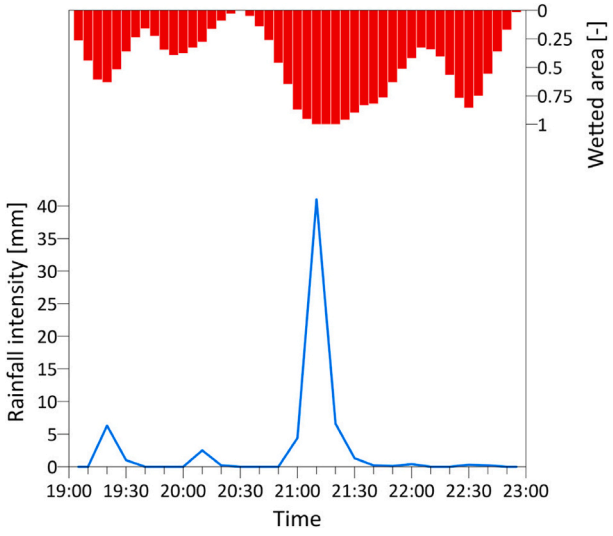

Fig. 5. Rainfall intensities (blue, as measured by the LSN rain gauge, for 10-min intervals) and wetted area (red, as recorded by the weather radar) of the storm that hit the city of Lausanne on June 11th, 2018.

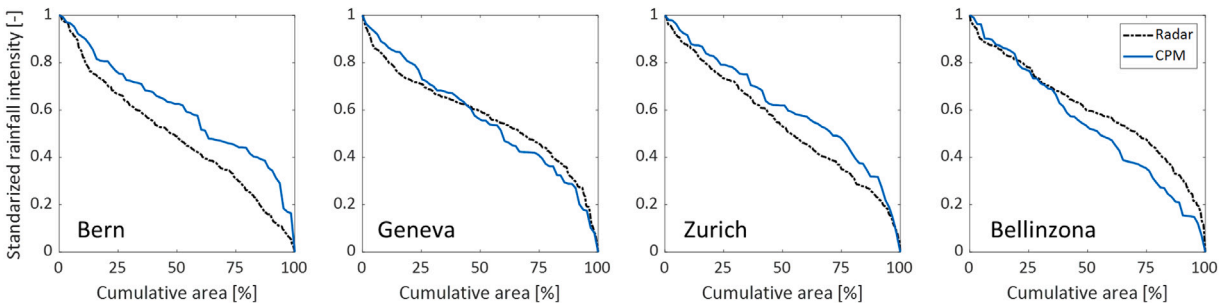

Fig. 6. The standardized rainfall spatial profiles of extreme storms as recorded by the weather radar (black dashed lines) and simulated by the CPM (blue solid lines) for the four cities.

3.2. Stochastic rainfall generator model

Stochastic rainfall generators are used to simulate extreme storms for flood assessments, especially in urban areas (McRobie et al., 2013; Peleg et al., 2017a). The models can be used to generate multiple storms with extreme rainfall events for a given climate or they can be used to generate individual extreme storms with a known return period. Storms simulated by gridded rainfall generators can be parameterized to reproduce the temporal structure of an observed extreme rainfall event, such as the storm duration and the temporal distribution of mean rainfall over the domain, but differ in the spatial distribution of rainfall intensities within the domain.

We simulated the design storm with the STREAP rainfall generator model (Paschalis et al., 2013), which was used in several climate impact studies in the past (Paschalis et al., 2014; Skinner et al., 2020; Peleg et al., 2020, 2021; Nyman et al., 2021; Ramirez et al., 2022, among others). We first obtained the information needed to stochastically generate a design storm that will have similar spatial characteristics of a real storm (i.e., a time series of $\hat{R}$, R_a, R_{cv}, and mean advection velocity and direction). These parameters can all be determined using weather radar data. Then, we used the Fast Fourier Transform method to simulate a Gaussian-mixture (bimodal) quantile field as we found that it enable a better representation of the convective structure of the rainfall. We allowed the quantile fields to advect and evolve over time using an auto-regressive moving average model (see Paschalis et al., 2013, for additional details). Last, we applied the inverse lognormal functions, as described in Section 2.1, to create rainfall-intensity fields from the quantile fields. We embedded the SQM, UQM and CC relation adjustment methods in the model to enable simulating the design storm for future climate conditions (Fig. 1), according to information obtained from CPM. The storm is simulated at a spatial resolution of 10 m x 10 m and temporal resolution of 5 min.

3.3. Convection-permitting model

We used convection-permitting climate simulations conducted with a horziontal grid spacing of 2.2 km over European domain (presented in Hentgen et al., 2019; Leutwyler et al., 2017). The simulations were conducted using the Consortium for Small-Scale Modeling in Climate Mode (COSMO-CLM) model (Baldauf et al., 2011) over 10 years long periods in present day climate driven by ERA-Interim reanalysis and future climate driven by pseudo-global-warming (PGW) approach (e.g. Schär et al., 1996; Rasmussen et al., 2011). The basic idea of the PGW approach is to apply large-scale perturbations (calculated as climate change signal from a General Circulation Model) at the lateral boundaries of a present-day simulation. The PGW simulations represent climate at the end of the century based on RCP8.5 greenhouse gas emission scenario.

First, we have investigated the CPM's capabilities to reproduce the spatial structure of extreme storms by comparing the storm profile of the 1% most intense rainfall fields obtained from the evaluation period of the CPM (for the years 1999–2009) with the radar data (2015–2019), assuming stationary climate for the 1999–2019 period. The rainfall spatial profiles represent the distribution of rainfall intensities according to their cumulative area, and they are computed for the rainfall composite as explained above. An illustration of the different types of rainfall spatial profiles, standardized from 0 (no rain) to 1 (peak intensity) to enable comparison between fields with different maximum rainfall intensities, is provided in Fig. S1. Since the lengths and periods of the sampled data differed as well as the space–time resolutions of the two products, we are not expecting a perfect match between the storm profiles, but we aimed to investigate if there was a general agreement between them. Still, it appears that the CPM simulates the rainfall spatial structure of extreme storms properly in the four cities, as there is a general agreement that storms exhibit spatial profiles between types 3 and 4 (Fig. 6).

Table 1
Scaling of rainfall variables $\hat{R}$ and R_a with temperature T [% °C^{-1}].

	Radar		CPM	
	$\hat{R}$	R_a	$\hat{R}$	R_a
Bern	4.3	−4.1	5.3	−5.4
Geneva	3.3	−2.5	3.5	−5.3
Zurich	2.4	−3.9	5.5	−5.1
Bellinzona	3.6	−1.5	1.5	−5.7

A second issue we examined was the validity of applying the "CC relation" adjustment, i.e., whether the scaling relationship between rainfall properties and temperature computed using CPM data is consistent with that of weather radar data. We calculated the scaling relationship between $\hat{R} - T$ and $R_a - T$ using the following equation:

$$log(R) = \alpha + \beta T, \tag{8}$$

where β is the regression coefficient (the scale) and T is the air temperature, bounded between 5 and 25 ^oC to avoid solid precipitation and the expected breaking point due to humidity limitations (Peleg et al., 2018). A 2 ^oC interval was used to bin the rainfall variables $\hat{R}$ and R_a (further details on the binning method are given by Ali et al., 2021). Note that other methods can be employed to extract the CC-scale (e.g. Visser et al., 2021). The results of this examination show a high level of agreement between the radar and CPM rainfall–temperature scaling (Table 1), as both show a strengthening of the storm ($\hat{R}$) and a decreasing area (R_a) with increasing temperature. All trends were found significant by the Mann–Kendall test (p-values$\ll$0.05); the fitting statistics are presented in Table S1.

3.4. Design storm modifications

The storm profiles of the 1% most intense rainfall fields for the present and future climates were obtained from the CPM for the four different domains (Fig. 7). These profiles were used as the basis for the SQM adjustment, along with the information of the change in the

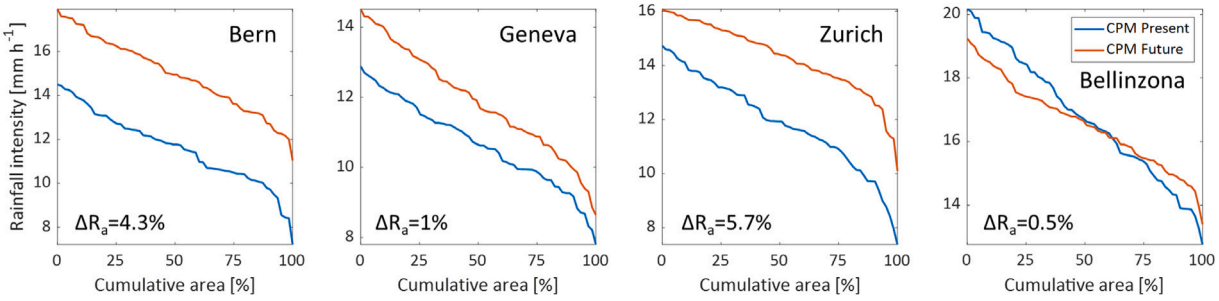

Fig. 7. Rainfall spatial profiles for the 1% most intense rainfall as simulated by the CPM for the present (blue lines) and future (red lines) climates for the four cities.

storm area (ΔR_a) in each of the locations. The example of the present and future storm composites and the changes to the storm profile in Fig. 2 was generated using the CPM information for Bern. In Fig. 8, four additional examples of simulated present and future storm composites for the Bern area are presented to illustrate the spatial stochasticity of the rainfall generator model and its potential to simulate multiple realizations of the same design storm. It is noteworthy that the area of the storm chosen in our case study to demonstrate the storm adjustment process is relatively small compared to the grid spacing of the CPM; we only have 256 grid cells for calculating the spatial composite of CPM's storms, which can lead to under-representation of the storm profile. CPM domains should be matched up with the storm extent to be adjusted and a sufficient number of grid cells should be available to accurately represent the storm spatial structure.

A change in 2-m air temperature during the occurrence of the 1% most intense rainfall simulated by the CPM for the present and future climates was computed ($\Delta T_{1\%}$) to modify the "Lausanne storm" according to the CC relation (Table 2). To apply the UQM method, the rainfall intensity quantiles for the present and future climates were extracted from the CPM for each location (see example in Fig. S2).

Table 2
Change in temperature during the occurrence of the 1% most intense rainfall.

	$\Delta T_{1\%}$
Bern	1.8
Geneva	1
Zurich	2
Bellinzona	1.1

3.5. Inundation model

The outputs of the rainfall generator model, i.e. the ensemble of simulated design storms both for present and future climates, were input into the CADDIES/CAFlood 2D cellular automata flood model (Guidolin et al., 2016). CADDIES provides data structures to store rasters and automata spaces, methods to retrieve and assign automaton cell neighborhoods, abstract methods to implement transition functions and more. CAFlood is an application for rapid flood modeling that has been widely used both in academic research (recent publications include Webber et al., 2020; Vamvakeridou-Lyroudia et al., 2020; Padulano et al., 2021, among many others) and in the private sector (see case studies in: https://www.cafloodpro.com/). The required inputs include terrain elevation, roughness, rainfall and water levels at domain boundaries. At each time step, CAFlood applies the Manning's equation in each automaton cell to compute the velocity of water flowing from/to each of its neighbors, to ultimately calculate the resulting water level in each cell. To this end, the edge between a cell and its neighbor is treated as a channel of width equal to cell side length. The version of the CADDIES/CAFlood model used in this study includes the possibility to take spatially distributed rainfall into account. Fig. 9 shows an example

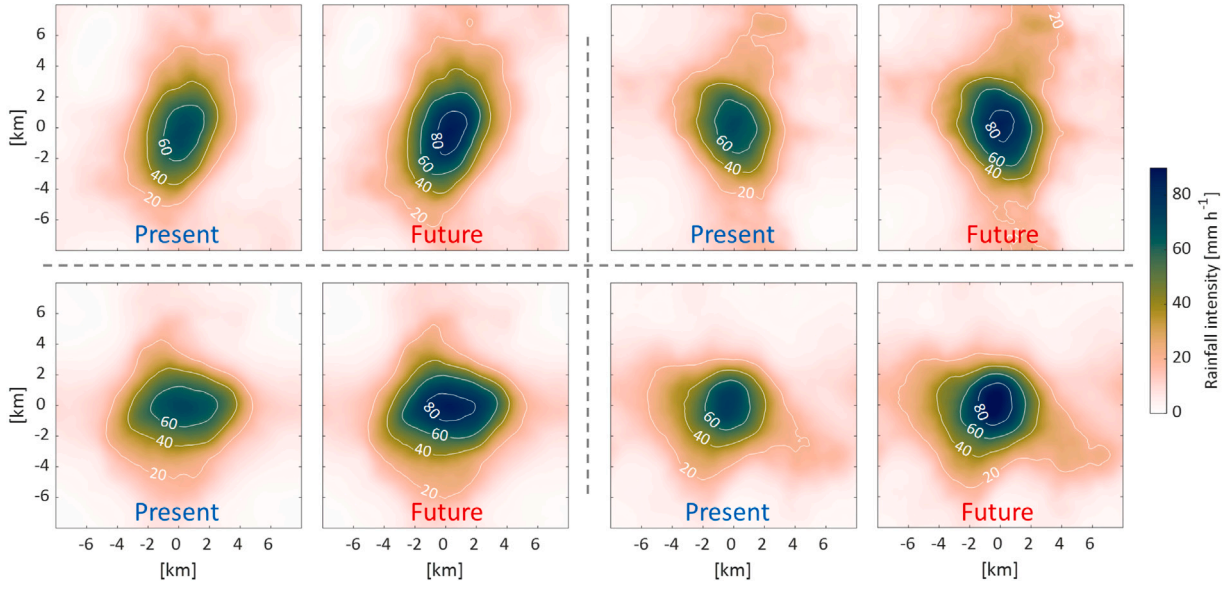

Fig. 8. An example of four storm composites, depicting the present and future "Lausanne storm" in Bern, simulated by the stochastic rainfall generator model and the SQM method using information from the CPM.

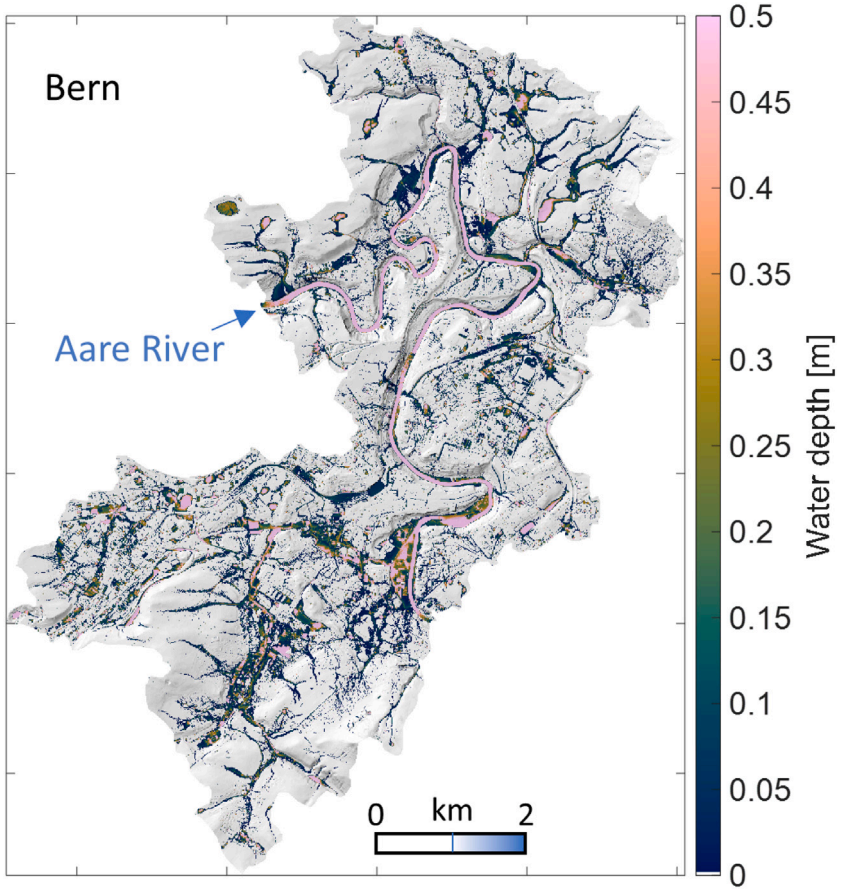

Fig. 9. An example of an inundation map generated by the CADDIES/CAFlood 2D cellular automata flood model, based on the STREAP model rainfall simulations. The map shows the average maximum water depths of 30 realizations of the "Lausanne storm" in the city of Bern representing the present climate.

of an inundation map produced by the model, showing the average maximum water depths of 30 realizations of the "Lausanne storm" (simulated for the present climate conditions) in the city of Bern.

From the results obtained using the inundation model, water depth maps at each time step were used for analyzing the impact of the different storm adjustment methods on the flood characteristics, which were summarized in two statistical measures. We first computed the ratio of change in peak water depths between the future scenarios and the rainfall-runoff simulations of the present:

$$\Delta h = \frac{\sum_{i=1}^{N} h_i^F - \sum_{i=1}^{N} h_i^P}{\sum_{i=1}^{N} h_i^P}, \tag{9}$$

where h_i is the water depth at any grid cell i, N is the total number of grid cells in the domain and P and F are the present and future (corrected method) simulations, respectively.

In addition, we calculated the ratio of change in the flooded area ($\Delta\theta$) between the present and future simulations. Grid cells i with a peak water depth above 10 cm were considered flooded and assigned a value of 1 (or 0 otherwise). Then, we used Eq. (9) to sum the flooded area, replacing h_i with θ_i.

3.6. The hydrological response to the rainfall adjustment

Different hydrological responses result from the three different storm adjustment methods, as expected. The SQM method is associated with higher water depths (Fig. 10) and larger inundated areas (Fig. S3) in Bern, Geneva, and Zurich. This can be explained by the increasing area of the storm and the increasing intensity of the rainfall in these locations (Fig. 7). However, in Bellinzona, the storm area is expected only to increase slightly, and the peak rainfall intensity is expected to weaken (Fig. 7), resulting in reduced hydrological impacts (Fig. 10 and S3). We note that in comparison to the other locations, CPM data for Bellinzona are less in agreement with radar data (Table 1). Another possibility could be that the limited data from future climate simulations (10 years) do not show extremely heavy rainfall storms in this region. The two homogeneous rain adjustment methods (UQM and CC relation) agree well in two locations, Bern and Zurich; contrary to this, the UQM has a much greater impact on flood assessments in Geneva and Bellinzona (Fig. 10 and S3).

3.7. Implications

It is evident from the results that it is essential to apply rainfall adjustment to both rainfall intensities and the spatial structure of storms as the impact on the flood can be significant. Spatial rainfall adjustment is more likely to be important in catchments with fast hydrological responses, such as small- to medium-sized rural catchments or urban areas, and less important in large catchments where the temporal structure of rainfall should be more influential; however, further research is needed to examine the impact of changes in convection organization on catchment response at large scales.

For this case study, the purpose of applying rainfall adjustments was not to identify the "true" signal of change in flood assessments for the four locations, but rather to demonstrate the SQM method. The assessment of climate change impacts on flood statistics and their uncertainties requires using additional climate scenarios and rainfall adjustment methods, and performing a detailed validation of the CPM's ability to represent rainfall for these locations, which is beyond the scope of this paper.

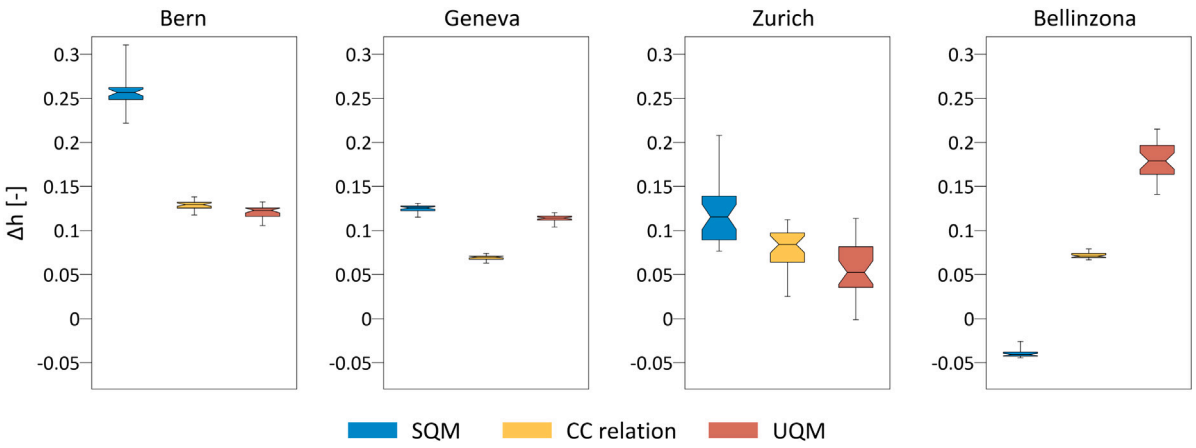

Fig. 10. The ratio of the change in the water depths between the present and future simulations (SQM — blue, CC relation — yellow, UQM — red). Each boxplot represents 30 realizations of the design storm, showing the median change (solid line), the 25th–75th percentile range (boxed area), and the minimum–maximum range (bounded with lines).

Furthermore, we demonstrated the SQM on a single convective storm, but it should be noted that the method can be applied to any type of storm, for example, stratiform storms. Research is still needed on how to identify the storm types in CPM and extract the adjustment factors, a task that remains challenging.

4. Perspectives on SQM's future development

Under the assumption that the rainfall structure and intensity will change the same throughout the storm duration, we demonstrated the spatial adjustment of design storms. Changes in rainfall structure, however, are likely to be non-stationary, hence we plan to further develop the SQM scheme to adjust design storms both spatially and temporally. Additionally, changes in the spatial structure of the storm are likely influenced by the type of rainfall (e.g. convective vs. stratiform), its source, and orientation. It is possible to address this issue if the changes to the spatial structure obtained from the CPM are analyzed based on rainfall types. In addition, the SQM properties (i.e. the change in storm area and the change in spatial quantile of rainfall intensity) can be scaled with the return period of extreme storms. The result will be a more flexible form of correction to design storms of varying severity.

5. Conclusions

We presented the SQM, a simple method for spatially adjusting the structure of design storms. Using data from a CPM, we applied the SQM to a design storm and presented a case study. Results indicate that modifying the spatial structure of the storm can yield considerable differences in flood impacts in comparison to other adjustment methods that apply uniform adjustment to rainfall intensities. We plan to extend SQM to adjust rainfall also in its temporal component in the future, in addition to the spatial component of the adjustment described in this paper.

Code availability

An example of the Spatial Quantile Mapping (SQM) method can be found in the Zenodo archive at https://doi.org/10.5281/zenodo.6563635. This script (Peleg, 2022) reproduces Fig. 3 from the manuscript.

CRediT authorship contribution statement

Nadav Peleg: Writing – original draft, Conceptualization, Methodology, Software, Writing – review & editing. **Nikolina Ban:** Writing – review & editing, Conceptualization. **Michael J. Gibson:** Writing – review & editing, Conceptualization, Software. **Albert S. Chen:** Writing – review & editing, Conceptualization. **Athanasios Paschalis:** Writing – review & editing, Conceptualization, Software. **Paolo Burlando:** Writing – review & editing, Conceptualization. **João P. Leitão:** Writing – original draft, Conceptualization, Methodology, Software.

Declaration of competing interest

The authors declare that they have no known competing financial interests or personal relationships that could have appeared to influence the work reported in this paper.

Acknowledgments

NP acknowledges the support of the Swiss National Science Foundation (SNSF), Grant 194649 ("Rainfall and floods in future cities"). NB acknowledges PRACE for awarding her access to Piz Daint at Swiss National Supercomputing Center (CSCS, Switzerland). NB also acknowledges the Federal Office for Meteorology and Climatology MeteoSwiss, the Swiss National Supercomputing Centre (CSCS), and ETH Zürich for their contributions to the development of the GPU-accelerated version of COSMO. ASC acknowledges the Alan Turning Institute for the support to his work via Turing Fellow at University of Exeter. CADDIES/CAFlood 2D was originally developed in the project Simplified Dual-Drainage Modelling for Flood Risk Assessment in Urban Areas (GR/J09796), funded by the UK Engineering and Physical Sciences Research Council.

Appendix A. Supplementary data

Supplementary material related to this article can be found online at https://doi.org/10.1016/j.advwatres.2022.104258.

References

Ali, H., Peleg, N., Fowler, H.J., 2021. Global scaling of rainfall with dewpoint temperature reveals considerable ocean-land difference. Geophys. Res. Lett. 48 (15), http://dx.doi.org/10.1029/2021GL093798, e2021GL093798.

Baldauf, M., Seifert, A., Förstner, J., Majewski, D., Raschendorfer, M., Reinhardt, T., 2011. Operational convective-scale numerical weather prediction with the cosmo model: description and sensitivities. Monthly Weather Rev. 139, 3887–3905. http://dx.doi.org/10.1175/MWR-D-10-05013.1.

Ban, N., Caillaud, C., Coppola, E., Pichelli, E., Sobolowski, S., Adinolfi, M., Ahrens, B., Alias, A., Anders, I., Bastin, S., et al., 2021. The first multi-model ensemble of regional climate simulations at kilometer-scale resolution, part I: evaluation of precipitation. Clim. Dynam. 57, 1–28. http://dx.doi.org/10.1007/s00382-021-05708-w.

Ban, N., Schmidli, J., Schar, C., 2014. Evaluation of the convection-resolving regional climate modeling approach in decade-long simulations. J. Geophys. Res.: Atmos. 119 (13), 7889–7907. http://dx.doi.org/10.1002/2014JD021478.

Ban, N., Schmidli, J., Schar, C., 2015. Heavy precipitation in a changing climate: Does short-term summer precipitation increase faster? Geophys. Res. Lett. 42 (4), 1165–1172. http://dx.doi.org/10.1002/2014GL062588.

Belachsen, I., Marra, F., Peleg, N., Morin, E., 2017. Convective rainfall in a dry climate: relations with synoptic systems and flash-flood generation in the Dead Sea region. Hydrol. Earth Syst. Sci. 21 (10), 5165–5180. http://dx.doi.org/10.5194/hess-21-5165-2017.

Berggren, K., Packman, J., Ashley, R., Viklander, M., 2014. Climate changed rainfalls for urban drainage capacity assessment. Urban Water J. 11 (7), 543–556. http://dx.doi.org/10.1080/1573062X.2013.851709.

Berk, M., Spackova, O., Straub, D., 2017. Probabilistic design storm method for improved flood estimation in ungauged catchments. Water Resour. Res. 53 (12), 10701–10722. http://dx.doi.org/10.1002/2017WR020947.

Bloeschl, G., Hall, J., Viglione, A., Perdigao, R.A.P., Parajka, J., Merz, B., Lun, D., Arheimer, B., Aronica, G.T., Bilibashi, A., Bohac, M., Bonacci, O., Borga, M., Canjevac, I., Castellarin, A., Chirico, G.B., Claps, P., Frolova, N., Ganora, D., Gorbachova, L., Gul, A., Hannaford, J., Harrigan, S., Kireeva, M., Kiss, A., Kjeldsen, T.R., Kohnova, S., Koskela, J.J., Ledvinka, O., Macdonald, N., Mavrova-Guirguinova, M., Mediero, L., Merz, R., Molnar, P., Montanari, A., Murphy, C., Osuch, M., Ovcharuk, V., Radevski, I., Salinas, J.L., Sauquet, E., Sraj, M., Szolgay, J., Volpi, E., Wilson, D., Zaimi, K., Zivkovic, N., 2019. Changing climate both increases and decreases European river floods. Nature 573 (7772), 108+. http://dx.doi.org/10.1038/s41586-019-1495-6.

Chen, Y., Paschalis, A., Kendon, E., Kim, D., Onof, C., 2021. Changing spatial structure of summer heavy rainfall, using convection-permitting ensemble. Geophys. Res. Lett. 48 (3), http://dx.doi.org/10.1029/2020GL090903, e2020GL090903.

Chimene, C.A., Campos, J.N.B., 2020. The design flood under two approaches: synthetic storm hyetograph and observed storm hyetograph. J. Appl. Water Eng. Res. 8 (3), 171–182. http://dx.doi.org/10.1080/23249676.2020.1787242.

Cho, H., Bowman, K., North, G., 2004. A comparison of gamma and lognormal distributions for characterizing satellite rain rates from the tropical rainfall measuring mission. J. Appl. Meteorol. 43 (11), 1586–1597. http://dx.doi.org/10.1175/JAM2165.1.

Fatichi, S., Ivanov, V.Y., Paschalis, A., Peleg, N., Molnar, P., Rimkus, S., Kim, J., Burlando, P., Caporali, E., 2016. Uncertainty partition challenges the predictability of vital details of climate change. Earth's Future 4 (5), 240–251. http://dx.doi.org/10.1002/2015EF000336.

Fowler, H.J., Lenderink, G., Prein, A.F., Westra, S., Allan, R.P., Ban, N., Barbero, R., Berg, P., Blenkinsop, S., Do, H.X., et al., 2021a. Anthropogenic intensification of short-duration rainfall extremes. Nature Rev. Earth Environ. 2 (2), 107–122. http://dx.doi.org/10.1038/s43017-020-00128-6.

Fowler, H.J., Wasko, C., Prein, A.F., 2021b. Intensification of short-duration rainfall extremes and implications for flood risk: current state of the art and future directions. Phil. Trans. R. Soc. A 379 (2195), 20190541. http://dx.doi.org/10.1098/rsta.2019.0541.

Germann, U., Boscacci, M., Gabella, M., Sartori, M., 2015. Peak performance: Radar design for prediction in the Swiss Alps. Meteorol. Technol. Int. 4, 42–45.

Guneralp, B., Guneralp, I., Liu, Y., 2015. Changing global patterns of urban exposure to flood and drought hazards. Global Environ. Change-Human Policy Dimens. 31, 217–225. http://dx.doi.org/10.1016/j.gloenvcha.2015.01.002.

Guidolin, M., Chen, A.S., Ghimire, B., Keedwell, E.C., Djordjeviac, S., Saviac, D.A., 2016. A weighted cellular automata 2D inundation model for rapid flood analysis. Environ. Model. Softw. 84, 378–394. http://dx.doi.org/10.1016/j.envsoft.2016.07.008.

Hentgen, L., Ban, N., Kroner, N., Leutwyler, D., Schar, C., 2019. Clouds in convection-resolving climate simulations over europe. J. Geophys. Res.: Atmos. 124 (7), 3849–3870. http://dx.doi.org/10.1029/2018JD030150.

Hirabayashi, Y., Mahendran, R., Koirala, S., Konoshima, L., Yamazaki, D., Watanabe, S., Kim, H., Kanae, S., 2013. Global flood risk under climate change. Nat. Clim. Change 3 (9), 816–821. http://dx.doi.org/10.1038/NCLIMATE1911.

Jongman, B., Hochrainer-Stigler, S., Feyen, L., Aerts, J.C.J.H., Mechler, R., Botzen, W.J.W., Bouwer, L.M., Pflug, G., Rojas, R., Ward, P.J., 2014. Increasing stress on disaster-risk finance due to large floods. Nat. Clim. Change 4 (4), 264–268. http://dx.doi.org/10.1038/NCLIMATE2124.

Lenderink, G., de Vries, H., Fowler, H.J., Barbero, R., van Ulft, B., van Meijgaard, E., 2021. Scaling and responses of extreme hourly precipitation in three climate experiments with a convection-permitting model. Phil. Trans. R. Soc. A 379 (2195), 20190544. http://dx.doi.org/10.1098/rsta.2019.0544.

Leutwyler, D., Lüthi, D., Ban, N., Fuhrer, O., Schär, C., 2017. Evaluation of the convection-resolving climate modeling approach on continental scales. J. Geophys. Res.: Atmos. 122 (10), 5237–5258. http://dx.doi.org/10.1002/2016JD026013.

Li, J., Wasko, C., Johnson, F., Evans, J.P., Sharma, A., 2018. Can regional climate modeling capture the observed changes in spatial organization of extreme storms at higher temperatures? Geophys. Res. Lett. 45 (9), 4475–4484. http://dx.doi.org/10.1029/2018GL077716.

Lind, P., Belušić, D., Christensen, O.B., Dobler, A., Kjellström, E., Landgren, O., Lindstedt, D., Matte, D., Pedersen, R.A., Toivonen, E., et al., 2020. Benefits and added value of convection-permitting climate modeling over Fenno-Scandinavia. Clim. Dynam. 55 (7), 1893–1912. http://dx.doi.org/10.1007/s00382-020-05359-3.

Lochbihler, K., Lenderink, G., Siebesma, A.P., 2017. The spatial extent of rainfall events and its relation to precipitation scaling. Geophys. Res. Lett. 44 (16), 8629–8636. http://dx.doi.org/10.1002/2017GL074857.

Mallakpour, I., Villarini, G., 2015. The changing nature of flooding across the central United States. Nat. Clim. Change 5 (3), 250–254. http://dx.doi.org/10.1038/NCLIMATE2516.

McRobie, F.H., Wang, L.-P., Onof, C., Kenney, S., 2013. A spatial-temporal rainfall generator for urban drainage design. Water Sci. Technol. 68 (1), 240–249. http://dx.doi.org/10.2166/wst.2013.241.

Molnar, P., Fatichi, S., Gaál, L., Szolgay, J., Burlando, P., 2015. Storm type effects on super Clausius-Clapeyron scaling of intense rainstorm properties with air temperature. Hydrol. Earth Syst. Sci. 19 (4), 1753–1766. http://dx.doi.org/10.5194/hess-19-1753-2015.

Moraga, J.S., Peleg, N., Fatichi, S., Molnar, P., Burlando, P., 2021. Revealing the impacts of climate change on mountainous catchments through high-resolution modelling. J. Hydrol. 603, 126806. http://dx.doi.org/10.1016/j.jhydrol.2021.126806.

Moustakis, Y., Onof, C.J., Paschalis, A., 2020. Atmospheric convection, dynamics and topography shape the scaling pattern of hourly rainfall extremes with temperature globally. Commun. Earth Environ. 1 (1), 1–9. http://dx.doi.org/10.1038/s43247-020-0003-0.

Moustakis, Y., Papalexiou, S.M., Onof, C.J., Paschalis, A., 2021. Seasonality, intensity, and duration of rainfall extremes change in a warmer climate. Earth's Future 9 (3), http://dx.doi.org/10.1029/2020EF001824, e2020EF001824.

Niemi, T.J., Guillaume, J.H.A., Kokkonen, T., Hoang, T.M.T., Seed, A.W., 2016. Role of spatial anisotropy in design storm generation: Experiment and interpretation. Water Resour. Res. 52 (1), 69–89. http://dx.doi.org/10.1002/2015WR017521.

Nyman, P., Yeates, P., Langhans, C., Noske, P.J., Peleg, N., Schärer, C., Lane, P.N.J., Haydon, S., Sheridan, G.J., 2021. Probability and consequence of postfire erosion for treatability of water in an unfiltered supply system. Water Resour. Res. 57 (1), http://dx.doi.org/10.1029/2019WR026185, 2019WR026185.

Olsson, J., Amaguchi, H., Alsterhag, E., Dåverhög, M., Adrian, P.-E., Kawamura, A., 2013. Adaptation to climate change impacts on urban storm water: A case study in Arvika, Sweden. Clim. Change 116 (2), 231–247. http://dx.doi.org/10.1007/s10584-012-0480-y.

Onof, C., Chandler, R., Kakou, A., Northrop, P., Wheater, H., Isham, V., 2000. Rainfall modelling using Poisson-cluster processes: a review of developments. Stoch. Environ. Res. Risk Assess. 14 (6), 384–411. http://dx.doi.org/10.1007/s004770000043.

Padulano, R., Rianna, G., Costabile, P., Costanzo, C., Del Giudice, G., Mercogliano, P., 2021. Propagation of variability in climate projections within urban flood modelling: A multi-purpose impact analysis. J. Hydrol. 602, 126756. http://dx.doi.org/10.1016/j.jhydrol.2021.126756.

Paprotny, D., Sebastian, A., Morales-Napoles, O., Jonkman, S.N., 2018. Trends in flood losses in Europe over the past 150 years. Nat. Commun. 9, http://dx.doi.org/10.1038/s41467-018-04253-1.

Paschalis, A., Fatichi, S., Molnar, P., Rimkus, S., Burlando, P., 2014. On the effects of small scale space-time variability of rainfall on basin flood response. J. Hydrol. 514, 313–327. http://dx.doi.org/10.1016/j.jhydrol.2014.04.014.

Paschalis, A., Molnar, P., Fatichi, S., Burlando, P., 2013. A stochastic model for high-resolution space-time precipitation simulation. Water Resour. Res. 49 (12), 8400–8417. http://dx.doi.org/10.1002/2013WR014437.

Peleg, N., 2022. Spatial quantile mapping code example. http://dx.doi.org/10.5281/zenodo.6563635.

Peleg, N., Blumensaat, F., Molnar, P., Fatichi, S., Burlando, P., 2017a. Partitioning the impacts of spatial and climatological rainfall variability in urban drainage modeling. Hydrol. Earth Syst. Sci. 21 (3), 1559–1572. http://dx.doi.org/10.5194/hess-21-1559-2017.

Peleg, N., Fatichi, S., Paschalis, A., Molnar, P., Burlando, P., 2017b. An advanced stochastic weather generator for simulating 2-D high-resolution climate variables. J. Adv. Modelling Earth Syst. 9 (3), 1595–1627. http://dx.doi.org/10.1002/2016MS000854.

Peleg, N., Marra, F., Fatichi, S., Molnar, P., Morin, E., Sharma, A., Burlando, P., 2018. Intensification of convective rain cells at warmer temperatures observed from high-resolution weather radar data. J. Hydrometeorol. 19 (4), 715–726. http://dx.doi.org/10.1175/JHM-D-17-0158.1.

Peleg, N., Morin, E., 2014. Stochastic convective rain-field simulation using a high-resolution synoptically conditioned weather generator (HiReS-WG). Water Resour. Res. 50 (3), 2124–2139. http://dx.doi.org/10.1002/2013WR014836.

Peleg, N., Shamir, E., Georgakakos, K.P., Morin, E., 2015. A framework for assessing hydrological regime sensitivity to climate change in a convective rainfall environment: a case study of two medium-sized eastern Mediterranean catchments, Israel. Hydrol. Earth Syst. Sci. 19 (1), 567–581. http://dx.doi.org/10.5194/hess-19-567-2015.

Peleg, N., Skinner, C., Fatichi, S., Molnar, P., 2020. Temperature effects on the spatial structure of heavy rainfall modify catchment hydro-morphological response. Earth Surface Dyn. 8 (1), 17–36. http://dx.doi.org/10.5194/esurf-8-17-2020.

Peleg, N., Skinner, C., Ramirez, J.A., Molnar, P., 2021. Rainfall spatial-heterogeneity accelerates landscape evolution processes. Geomorphology 390, 107863. http://dx.doi.org/10.1016/j.geomorph.2021.107863.

Prein, A.F., Langhans, W., Fosser, G., Ferrone, A., Ban, N., Goergen, K., Keller, M., Tölle, M., Gutjahr, O., Feser, F., Brisson, E., Kollet, S., Schmidli, J., van Lipzig, N.P.M., Leung, R., 2015. A review on regional convection-permitting climate modeling: Demonstrations, prospects, and challenges. Rev. Geophys. 53 (2), 323–361. http://dx.doi.org/10.1002/2014RG000475.

Prein, A.F., Liu, C., Ikeda, K., Bullock, R., Rasmussen, R.M., Holland, G.J., Clark, M., 2020. Simulating North American mesoscale convective systems with a convection-permitting climate model. Clim. Dynam. 55 (1), 95–110. http://dx.doi.org/10.1007/s00382-017-3993-2.

Prein, A.F., Liu, C., Ikeda, K., Trier, S.B., Rasmussen, R.M., Holland, G.J., Clark, M.P., 2017. Increased rainfall volume from future convective storms in the US. Nature Clim. Change 7 (12), 880–884. http://dx.doi.org/10.1038/s41558-017-0007-7.

Ramirez, J.A., Mertin, M., Peleg, N., Horton, P., Skinner, C., Zimmermann, M., Keiler, M., 2022. Modelling the long-term geomorphic response to check dam failures in an alpine channel with CAESAR-Lisflood. Int. J. Sediment Res. http://dx.doi.org/10.1016/j.ijsrc.2022.04.005.

Rasmussen, R., Liu, C., Ikeda, K., Gochis, D., Yates, D., Chen, F., Tewari, M., Barlage, M., Dudhia, J., Yu, W., Miller, K., Arsenault, K., Grubišić, V., Thompson, G., Gutmann, E., 2011. High-resolution coupled climate runoff simulations of seasonal snowfall over colorado: A process study of current and warmer climate. J. Clim. 24 (12), 3015–3048. http://dx.doi.org/10.1175/2010JCLI3985.1.

Schär, C., Frei, C., Lüthi, D., Davies, H.C., 1996. Surrogate climate-change scenarios for regional climate models. Geophys. Res. Lett. 23 (6), 669–672. http://dx.doi.org/10.1029/96GL00265.

Schär, C., Fuhrer, O., Arteaga, A., Ban, N., Charpilloz, C., Girolamo, S.D., Hentgen, L., Hoefler, T., Lapillonne, X., Leutwyler, D., Osterried, K., Panosetti, D., Rüdisühli, S., Schlemmer, L., Schulthess, T.C., Sprenger, M., Ubbiali, S., Wernli, H., 2020. Kilometer-scale climate models: prospects and challenges. Bull. Am. Meteorol. Soc. 101, E567 – E587. http://dx.doi.org/10.1175/BAMS-D-18-0167.1.

Singer, M.B., Michaelides, K., Hobley, D.E.J., 2018. STORM 1.0: a simple, flexible, and parsimonious stochastic rainfall generator for simulating climate and climate change. Geosci. Model Dev. 11 (9), 3713–3726. http://dx.doi.org/10.5194/gmd-11-3713-2018.

Skinner, C.J., Peleg, N., Quinn, N., Coulthard, T.J., Molnar, P., Freer, J., 2020. The impact of different rainfall products on landscape modelling simulations. Earth Surface Process. Landforms 45 (11), 2512–2523. http://dx.doi.org/10.1002/esp.4894.

Sun, S., Djordjevic, S., Khu, S.-T., 2011. A general framework for flood risk-based storm sewer network design. Urban Water J. 8 (1), 13–27. http://dx.doi.org/10.1080/1573062X.2010.542819.

Trenberth, K.E., 2011. Changes in precipitation with climate change. Clim. Res. 47 (1-2), 123–138. http://dx.doi.org/10.3354/cr00953.

Trenberth, K.E., Dai, A., Rasmussen, R.M., Parsons, D.B., 2003. The changing character of precipitation. Bull. Am. Meteorol. Soc. 84 (9), 1205–1218. http://dx.doi.org/10.1175/BAMS-84-9-1205.

Vamvakeridou-Lyroudia, L., Chen, A., Khoury, M., Gibson, M., Kostaridis, A., Stewart, D., Wood, M., Djordjevic, S., Savic, D., 2020. Assessing and visualising hazard impacts to enhance the resilience of critical infrastructures to urban flooding. Sci. Total Environ. 707, 136078. http://dx.doi.org/10.1016/j.scitotenv.2019.136078.

van den Boomgaard, R., van Balen, R., 1992. Methods for fast morphological image transforms using bitmapped binary images. CVGIP: Graph. Models Image Process. 54 (3), 252–258. http://dx.doi.org/10.1016/1049-9652(92)90055-3.

Visser, J.B., Wasko, C., Sharma, A., Nathan, R., 2021. Eliminating the hook in precipitation-temperature scaling. J. Clim. 34 (23), 9535–9549. http://dx.doi.org/10.1175/JCLI-D-21-0292.1.

Wasko, C., Sharma, A., 2015. Steeper temporal distribution of rain intensity at higher temperatures within Australian storms. Nat. Geosci. 8 (7), 527–529. http://dx.doi.org/10.1038/ngeo2456.

Wasko, C., Sharma, A., Westra, S., 2016. Reduced spatial extent of extreme storms at higher temperatures. Geophys. Res. Lett. 43 (8), 4026–4032. http://dx.doi.org/10.1002/2016GL068509.

Webber, J.L., Fletcher, T.D., Cunningham, L., Fu, G., Butler, D., Burns, M.J., 2020. Is green infrastructure a viable strategy for managing urban surface water flooding? Urban Water J. 17 (7), 598–608. http://dx.doi.org/10.1080/1573062X.2019.1700286.

Westra, S., Fowler, H.J., Evans, J.P., Alexander, L.V., Berg, P., Johnson, F., Kendon, E.J., Lenderink, G., Roberts, N.M., 2014. Future changes to the intensity and frequency of short-duration extreme rainfall. Rev. Geophys. 52 (3), 522–555. http://dx.doi.org/10.1002/2014RG000464.